Detecting Forest Fires in Southwest China From Remote Sensing Nighttime Lights Using the Random Forest Classification Model

Yuehan Yu, Lili Liu, Zhijian Chang, Yuanqing Li, and Kaifang Shi, *Member, IEEE*

***Abstract*—Forest fires are one of the most common natural disasters and public crisis events, presenting a serious threat to the ecosystem and human security. The traditional forest fire monitoring is time-consuming and inaccurate, but nighttime light remote sensing is enhancing the efficiency and speed of forest fire detection. Thus, this study focused on forest fire detection in Southwest China that was affected by fires in 2021 and 2022 using daily remote sensing nighttime light data from the black marble product VNP46A2 of the Suomi National Polar-Orbiting Partnership-Visible Infrared Imaging Radiometer Suite. Multiple features were developed based on the temporal features of day-level nighttime light radiances, which were divided into black pixels, stable light pixels, and forest fire pixels using the random forest classification model. To verify the accuracy, a confusion matrix was constructed to calculate the accuracy of the forest fire identification results by combining multisource data, and the results were compared with the results of different machine learning models and fire products. Moreover, the spatiotemporal distribution of forest fires was analyzed using trend analysis and nearest-neighbor analysis. Results show that the overall accuracy of pixel classification was over 92% in both years, with forest fire pixels classified with user's accuracy exceeding 99%. The forest fires were mainly dispersed and concentrated around the stable light pixels 400–700 m, and the distribution in different regions showed obvious spatial heterogeneity. Compared with 2021, the distribution of forest fires decreased significantly in 2022. This study can support the future management and protection of forest resources and the prediction of fire disasters. The dataset (2021 and 2022) of forest fires in Southwest China is available free of charge.[1]**

***Index Terms*—Forest fires, nighttime lights (NTLs), random forest classification, Southwest China, spatiotemporal analysis.**

I. Introduction

FOREST fires spread and expand unchecked within forested lands without human control, causing harm and losses to forests and humans [1], [2]. This type of natural disaster is sudden, destructive, and often difficult to control and mitigate [3]. Generally, forest fires can be broadly categorized into crown fires, surface fires, and underground fires [4], [5]. These classifications are based on the central location of the burning, the speed of the spread, the parts affected, and the intensity, with each type typically accompanied by the release of heat and smoke. The presence of fires on the ground, such as in crown or surface fires, is an important indicator of a fire's distribution and spread. Thus, forest fires are recognized as one of the most severe natural disasters and public crisis events in the international arena. They not only threaten human lives and property [6] but also exert a profound impact on the ecological environment and climate change [7], [8]. Moreover, as forest fires damage forest ecosystems, they also worsen carbon dioxide emissions, deteriorating the global ecological environment [9].

In traditional forest fire monitoring, manual patrols are dangerous, time-consuming, and laborious; monitoring data are scattered and untimely; and predictions are inaccurate. In addition, UAV monitoring equipment has a high cost, short endurance, a small cruising range, and power supply difficulties in alpine environments. It is also complex to maintain, has limited coverage, and has shortcomings, such as difficulties in discovery and localization, and an inability to judge fire situations [10], [11]. The monitoring of forest fires has been revolutionized with the advent of remote sensing technology [12], which allows remote sensing satellites to monitor and analyze the occurrence of forest fires (especially surface fires) in real time [13]. This is achieved by collecting daily remote sensing images of forested areas for the purpose of detecting and identifying targets and obtaining large-scale surface information. However, the limitations of climate, cloud cover, and sun angle add to the difficulty of daytime forest fire identification and monitoring using traditional visible-light remote sensing. Fortunately, the emerging nighttime light (NTL) remote sensing technology is providing additional convenience for the rapid and effective identification of forest fires [14], [15]. NTL can be used to analyze and detect areas of abnormal light brightness by

Manuscript received 7 April 2024; revised 23 May 2024; accepted 30 May 2024. Date of publication 6 June 2024; date of current version 14 June 2024. This work was supported in part by the National Natural Science Foundation of China under Grant 42101345, in part by the Natural Science Research Program of Anhui Universities under Grant 2023AH020029, and in part by the Special Fund for Youth Team of Southwest University under Grant SWU-XJLJ202305. *(Corresponding authors: Kaifang Shi; Yuanqing Li.)*

Yuehan Yu and Yuanqing Li are with the Chongqing Jinfo Mountain Karst Ecosystem National Observation and Research Station, School of Geographical Sciences, Southwest University, Chongqing 400715, China (e-mail: yyh164831@163.com; xslyq@foxmail.com).

Lili Liu and Zhijian Chang are with the School of Geographical Sciences, Southwest University, Chongqing 400715, China (e-mail: lll20010422@email.swu.edu.cn; pdszjchang@gmail.cn).

Kaifang Shi is with the Key Laboratory of Earth Surface Processes and Regional Response in the Yangtze-Huaihe River Basin, Anhui Province, School of Geography and Tourism, Anhui Normal University, Wuhu 241002, China (e-mail: shikf@ahnu.edu.cn).

Digital Object Identifier 10.1109/JSTARS.2024.3410172

[1][Online]. Available: https://doi.org/10.7910/DVN/QIUAE3

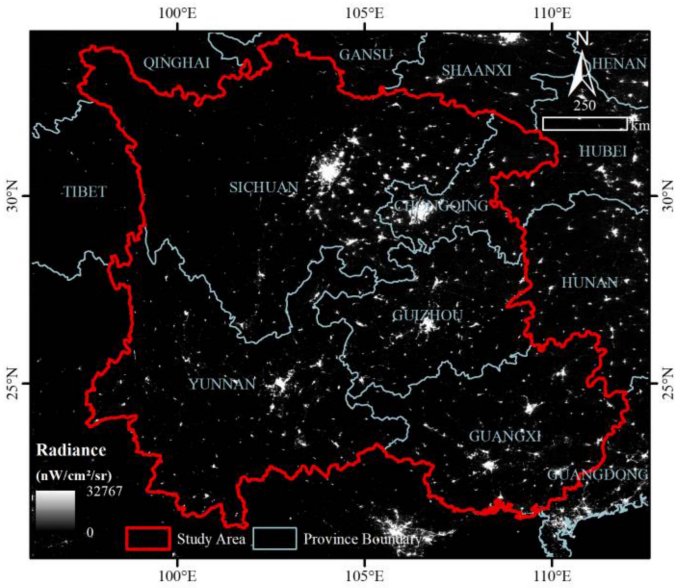

Fig. 1. Spatial locations of five provinces with NTLs in Southwest China.

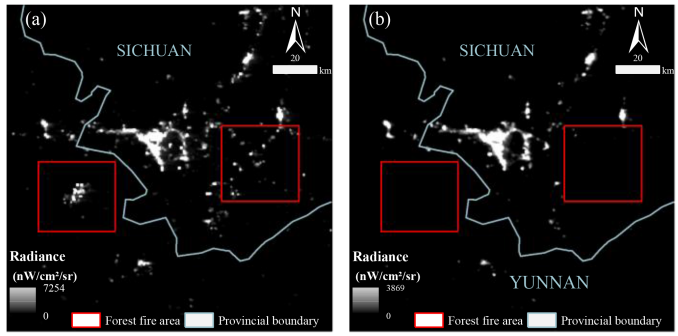

Fig. 2. Comparisons of NTL images. (a) Within the time window. (b) Outside the time window.

monitoring fire-generated hotspots or flames at night to detect signs of fire in a timely manner [16], thus providing more accurate and rapid fire monitoring and early warnings [17], [18].

The prerequisite for identifying forest fires (open fire component) using NTL data is classifying the images accurately. However, conventional machine learning models, such as decision trees and support vector machines, have issues, such as high computational demand, complex operation, and low accuracy [19], [20]. In comparison, the random forest classification model provides a superior approach to classifying remote sensing images [21], [22]. Random forest is an integrated multiclassifier machine learning model based on decision trees [23]. It can effectively reduce the generalization error of classification and simplify the design of classifiers. This model uses the classification and regression trees (CARTs) as the basis for tree building and improves prediction accuracy by combining multiple decision trees [20], [24]. Compared with a single decision tree, it effectively reduces the risk of overfitting and improves the tolerance of data outliers. With its fast training speed and strong resistance to overfitting, random forest is suitable for datasets with a large number of unknown features [25]. It is extremely popular in the field of remote sensing image classification and change detection [26], such as for ecosystem and land use classification [27], [28].

Based on the above analysis, this study takes Southwest China as the research object, introduces a random forest classification model to identify forest fires (open fire component) based on NTL images, and explores the spatial and temporal evolution trend of forest fires (see Fig. 1). A fire dataset for Southwest China has been constructed to provide important reference information and research support for decision-making departments. This dataset can be used to develop fire prevention and control strategies, establish prediction models, and manage and protect forest resources. The significance of this study extends to fire disaster prediction, risk assessment, and the establishment of an emergency response system, all of which contribute to the protection of national ecological security and sustainable development. The forest fires dataset is available.[2]

II. Study Area and Data Sources

A. Study Areas

Southwest China is an extremely forest-rich region that has been suffering from the threat of forest fires for many years and was, therefore, chosen as the study area [29]. The study area includes Sichuan, Chongqing, Guizhou, Guangxi, Yunnan, and Tibet autonomous region (TAR) (see Fig. 1). Climatically, the region features diverse climate types, such as subtropical monsoon, subtropical highland monsoon, and the distinctive plateau climate of the Tibetan plateau. The subtropical plateau monsoon climate is characterized by distinct wet and dry seasons, with a dry season lasting from November to April each year. During this time, it is difficult for cold northern air to converge with warm, humid air currents, leading to scant rainfall. In addition, temperatures rise and windy conditions prevail in March and April, creating a highly flammable and diverse forest landscape at increased risk of forest fires [30], [31]. Consequently, the forest fire prevention period in Southwest China tends to occur from November to April. This study focuses on five provinces in the region, excluding the TAR due to a lack of data.

B. Data Sources

NTL data: The VNP46A2 was used as the primary data source in this study (see Fig. 2). This is a day-level night product from NASAs Black Marble program within the VNP46 product suite. The VNP46A2 comprises seven layers that provide daily images of NTL radiation and corresponding quality control information with a spatial resolution of 15 arcsec. To ensure data quality, the VNP46A2 undergoes routine corrections for lunar bidirectional reflectance distribution function (BRDF), clouds [32], topography, atmosphere, airglow, and stray light, and includes a sensitivity enhancement for low-illumination structures [33]. This minimizes biases from extraneous artifacts,

[2][Online]. Available: https://doi.org/10.7910/DVN/QIUAE3

such as lunar radiance, in our analysis [34]. The gap-filled DNB BRDF-corrected NTL layer of the VNP46A2 accurately reflects the intensity of surface light sources and was used to construct the NTL characteristics of the pixels in this study. In this dataset, a background value of 65 535 nW/cm^2/sr was removed due to the presence of background values in the data. The mandatory quality flag within the VNP46A2 dataset was used to identify high-quality NTL pixels. For this study, gap layer data were corrected using quality layer data to filter valid pixels. Both layers were stored in HDF5 format. After batch conversion to GEOTIFF format, the images within the desired range were spliced and cropped to the study area's extent for the selection of high-quality NTL pixels. The data from two consecutive years, 2021 and 2022, were selected based on the occurrence of forest fires in Southwest China. The period from November to April of each year was established as the time window for this study.

Land use coverage data: We selected GlobeLand30 data, the world's first 30 m resolution global land cover product developed by China. This product provides a visual representation of the spatial distribution and information on the geographic location, range, and landscape pattern of ten types of land cover: cropland, forests, grasslands, scrublands, water bodies, wetlands, tundra, man-made surfaces, bare ground, glaciers, and permanent snow. The GlobeLand30 product has undergone rigorous validation and comparisons with similar products, ensuring a high level of accuracy and reliability [35]. The National Center for Basic Geographic Information (NCBGI) has released data for three periods: 2000, 2010, and 2020. We selected the 2020 dataset for our study. The 2020 dataset offers a spatial resolution of 30 m, with an overall accuracy of 85.72% and a Kappa coefficient of 0.82. It was reprojected to the WGS-84 coordinate system, and the land cover types of forest and shrub were specifically extracted for use in this research.

Administrative division data: The administrative division vector data of Southwest China in this study were obtained from the NCBGI.[3]

III. Methodology

The experimental process of this study was divided into four main parts (see Fig. 3). The first step involves preprocessing the data and filtering the Suomi National Polar-Orbiting Partnership-Visible Infrared Imaging Radiometer Suite (SNPP-VIIRS) data within the forest area. The second step is the identification of forest fires using the random forest classification model based on the screened night light data. The third step entails verifying the accuracy of the classification results. The fourth step is the spatial–temporal distribution analysis of forest fires.

A. Forest Fire Identification Based on the Random Forest Model

1) Training Sample Selection: This experimental study focused solely on forest areas to mitigate the confounding effect of artificial surface hotspots. Utilizing the Globalland30 product's

[3][Online]. Available: https://www.ngcc.cn/ngcc/

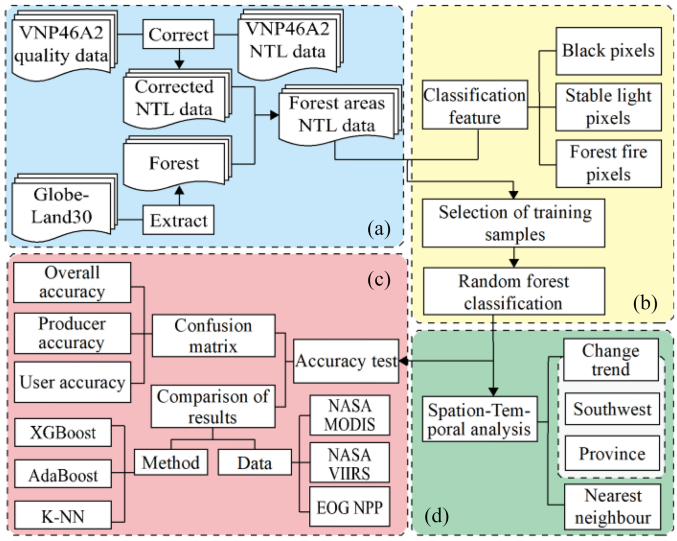

Fig. 3. Flowchart of detecting forest fires in Southwest China: (a) data preprocessing; (b) forest fire identification; (c) accuracy verification; (d) spatial-temporal distribution analysis.

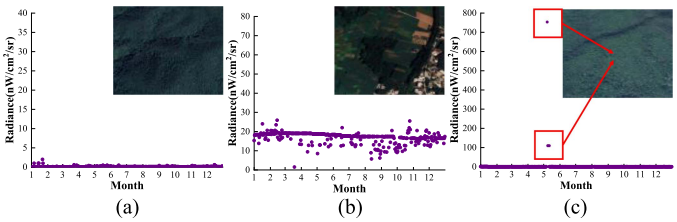

Fig. 4. Comparisons of Google Earth images with NTL radiance time series in a year of the three types of pixels: (a) black pixels; (b) stable light pixels; and (c) forest fire pixels.

2020 data, we screened for pixels where forests and shrubs constitute more than 20% of each pixel at the SNPP-VIIRS product's resolution [36]. This approach helped to exclude light and heat events originating from urban fires, ensuring that the identified black pixels, stable light pixels, and forest fire pixels accurately reflected the actual scene. In this study, we first preprocessed day-level NTL imagery throughout the year and constructed a time series of radiance to exclude unqualified data from the quality check and ensure the continuity and reliability of the time series. Should any pixels fail the quality check on specific dates, their values in the radiance time series were nullified to preserve data integrity and accuracy.

Based on the characteristics and radiance variation of nighttime lights in Southwest China over two years, they can be divided into three types: forest fire pixels, stable light pixels, and black pixels. Fig. 4 shows the changes in radiance on the NTL image of the three types of pixels over the course of a year, as well as the images of the three types of pixels on the Google Earth image. Forest fire pixels have zero or slightly greater than zero NTL radiance for most of the years, with unusually high NTL radiance values occurring only from November to April of each year. A sudden spike in NTL radiance is generally indicative of

TABLE I
CORRELATION ANALYSIS RESULTS BETWEEN NTL DATA AND VARIOUS SOCIOECONOMIC DATA

Data Source	Name	Description	Unit
VNP46 A2 Day-Level NTL Image	Maximum NTL Radiance (F_1)	Maximum NTL radiance of a pixel within a year	nW/cm²/sr
	Proportion of NTL Radiance Greater than Threshold (F_2)	The proportion of the number of days within a year when the NTL radiance of a pixel is greater than the threshold to the total number of days with effective values	/
	Mutation Rate of NTL Radiance (F_3)	The change rate of the maximum radiance of pixels in the forest fire time window relative to the maximum radiance outside the window	/

an ongoing forest fire at the pixel's location, which assists in pinpointing areas where forest fires have occurred. The radiance of stable light pixels remains consistently high throughout the year. Given that the selected area of NTL coverage encompasses over 20% of the forest in each pixel, and not all areas within a pixel are forested, the stable light pixels likely correspond to human activity zones, such as houses, roads, and protection stations. Consequently, this characteristic can be utilized to identify the areas of human activity, such as roads and houses, within forests. Black pixels exhibit almost zero brightness year round with no significant fluctuations, corresponding predominantly to forest regions devoid of human activity and forest fires, as well as some areas of bare land and water bodies.

Considering the unique characteristics of these three types of NTL pixels, we designed three key classification features for analyzing luminous images. They are maximum NTL radiance (F_1), proportion of NTL radiance greater than threshold (F_2), and mutation rate of NTL radiance (F_3), all of which are demonstrated in Table I.

The formula for calculating the maximum NTL radiance (F_1) is given as follows:

$$F_1 = \max\{r_1, r_2, \ldots, r_n\} \tag{1}$$

where n represents the number of days within a year that the NTL image pixel passed the quality screening, and $r_1, r_2, \ldots, r_n$ represent the NTL radiance values of the pixel within a year. Utilizing the land use data and Google Earth images, regions characterized by minimal human intervention were chosen, including forests, barren terrain, and aquatic zones within the designated forest pixels. Through comparative calculations, it is found that the maximum values of NTL radiance values in such areas for one year are all less than 0.5 nW/cm^2/sr, which is close to 0. This can effectively identify the black pixels and differentiate them from the forest fire pixels and stable light pixels.

The formula for calculating the proportion of NTL radiance greater than threshold (F_2) is given as follows:

$$F_2 = \frac{n'}{n} \tag{2}$$

where n represents the number of days in a year that the NTL image pixels passed the quality screening, and n' represents the number of days within a year that the NTL image pixels have an NTL radiance value greater than the threshold value. The areas with human activities, such as roads and houses in the forest, were selected based on the land use data and Google Earth images, and by comparing and calculating the threshold value set to 1 nW/cm^2/sr, it was found that the NTL radiance values of this type of pixels were more stable and were maintained at a higher level. The black pixels have lower NTL radiance values, the forest fire pixels are greater than the threshold value for fewer days, and the F_2 values approach 0, while the F_2 values of the stable light pixels are close to 1. Therefore, the stable light pixels can be effectively identified and differentiated from the black pixels and the forest fire pixels.

The formula for calculating the mutation rate of NTL radiance (F_3) is given as follows:

$$F_3 = \begin{cases} \frac{r_{\text{in}} - r_{\text{out}}}{r_{\text{out}}} & r_{\text{out}} > 0 \\ 0 & r_{\text{in}} = 0 \;\&\; r_{\text{out}} = 0 \\ r_{\text{in}} & r_{\text{in}} > 0 \;\&\; r_{\text{out}} = 0 \end{cases} \tag{3}$$

where r_{in} indicates the maximum value of the pixel within the forest fire time window, and r_{out} indicates the maximum value of the pixel outside the forest fire time window. When NTL pixels only show abrupt changes within the forest fire time window, they result in a higher F_3 value. When the NTL radiance value remains relatively stable throughout a year, the F_3 values approach 0. The forest fire pixels have larger F_3 values due to fires occurring within the forest fire time window, which results in sudden increases and decreases in the NTL radiance value. This allows the forest fire pixels to be effectively identified and differentiated from the black and stable light pixels.

2) Forest Fire Recognition: Our study delineated three pixel categories—black pixels, stable light pixels, and forest fire pixels—within five provinces of Southwest China using a combination of NTL data, GlobeLand30 land cover data, and Google Earth imagery. During the identification process, pixels consistently exhibiting radiance brightness values of less than 1 nW/cm^2/sr throughout the year were designated as surrogate black pixels. Conversely, pixels with daily radiance brightness values exceeding 5 nW/cm^2/sr were categorized as proxies for stable light pixels. Moreover, pixels with radiance brightness values higher than 5 nW/cm^2/sr and lower than 1 nW/cm^2/sr during the time window of the forest fires were primed as alternative forest fire pixels. We conducted a manual interpretation and filtering of the pixel categories with Google Earth imagery. Our criteria ensured that the land cover under black and forest fire pixels comprised more than 20% forested areas, while stable light pixels not only exhibited the same percentage of forest coverage but also included anthropogenic surface features, such as

TABLE II
PARAMETERS OF RANDOM FOREST CLASSIFICATION

Name	Description
BootStrap	whether to use bootstrap resampling
Estimators	Number of decision trees
MaxDepth	Maximum depth of the tree
MinSamplesLeaf	Minimum number of samples for leaf nodes
MinSamplesSplit	Minimum number of samples required for node splitting

roads and built-up regions. After screening, our training dataset consisted of 2500 samples for each pixel class: black pixels, stable light pixels, and forest fire pixels. For every filtered pixel class, we computed the maximum NTL radiance, the proportion of NTL radiance greater than the threshold, and the mutation rate of NTL radiance. These three characteristic values were ascribed to each pixel to ascertain its class affiliation, thereby establishing a training sample dataset poised for the random forest classification (see Table II).

The process of image classification using the random forest classification involves the following fundamental steps [37].

1) In the original sample, N training samples are randomly and repetitively drawn using the Bootstrap sampling method. One is drawn each time, forming a training sample set. Based on the extracted training sample sets, N CART decision trees are established, comprising a random forest. When each sample has M attributes at each node of the decision tree that needs to be split, m attributes are randomly selected from these M attributes, satisfying the condition $m << M$. Subsequently, from these m attributes, a strategy, such as information gain or Gini impurity, is employed to choose one attribute as the splitting attribute for the node.
2) The above step is repeated until the predetermined number of decision trees N has been created. The random forest classification model is established using the generated multitude of decision trees, which is then used to classify data and determine the categories of new samples. The model's performance is optimized by adjusting parameters, such as the number of trees, the maximum depth of the trees, and the minimum number of samples required to split a node. The predictive performance of the model is evaluated using methods, such as cross validation, and the optimal combination of parameters is selected based on this evaluation.

In the conducted experiment, the random forest classification prediction was executed utilizing the Scikit-Learn library to ascertain the categories of unlabeled data. The ensemble was configured with ten trees to facilitate bootstrap resampling during the forest construction phase, ensuring ample sample sizes for each tree and bolstering generalization capabilities.

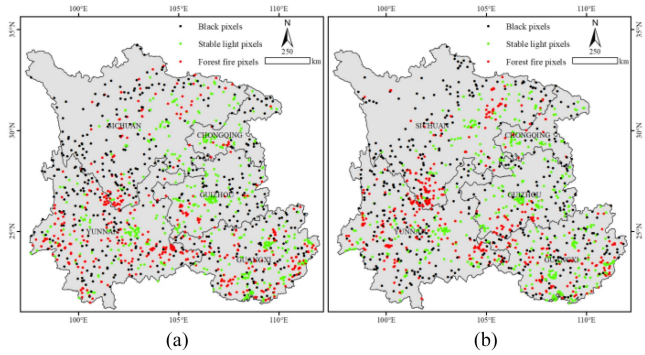

Fig. 5. Distribution of accuracy of test samples. (a) 2021. (b) 2022.

In addition to the configurations mentioned, default parameter settings, such as the node splitting criterion, were also employed.

B. Precision Testing

To guarantee the dependability and precision of the classification outcomes, this study incorporated a systematic series of verification procedures. These procedures leveraged an integration of NTL imagery and land cover datasets, and established instances of typical forest fires to assess the efficacy of the study's classification models in real-world scenarios.

A random assortment of samples was selected from the classification outcomes of each of the five provinces. These samples comprised three distinct categories and were evenly distributed across the years 2021 and 2022. After extraction, the sample order was randomized to reduce possible bias during the subsequent manual assessment process (see Fig. 5). Manual visual evaluation of the classification outcomes was conducted using the radiance time series from VNP46A2 day-level NTL images and corroborated using Google Earth images and GlobeLand30 land cover data. Pixels exhibiting NTL radiance near 0 without marked fluctuations over a year, and with over 20% of their area covered by forest and shrubbery—as confirmed by Google Earth—were classified as black pixels. Pixels with consistently high NTL radiance for a year, occupying more than 20% forest and shrub coverage, and corresponding to forested terrain with roads or built-up areas in Google Earth imagery, were identified as stable light pixels. Pixels that exhibited a significant increase in NTL radiance during the specific time window, with more than 20% of their area covered by forest and shrubland as verified using Google Earth, were classified as forest fire pixels. Samples that were ambiguous and could not be accurately classified based on the data were deemed invalid and excluded from the accuracy evaluation.

Ultimately, a confusion matrix was constructed using the statistical outcomes of the classification and the pixel count for each category. Subsequently, user accuracy, producer accuracy, and overall accuracy were computed to evaluate the precision of the classification outcomes and to demonstrate the efficacy of the classification model.

Post classification using the random forest approach, the derived data were compared with the results generated by eXtreme Gradient Boosting (XGBoost) [38], K-Nearest Neighbor

(K-NN) [39], [40], and Adaptive Boosting (AdaBoost) [41], as well as with NASA moderate-resolution imaging spectroradiometer (MODIS) [42], visible infrared imaging radiometer suite (VIIRS) [43], and the Earth Observation Group (EOG) National Polar-Orbiting Partnership (NPP) fire point products [44], to validate the superiority of the random forest model in this experiment [45].

C. Spatiotemporal Analysis of Forest Fires

1) Change Trend Analysis: The change trend analysis was used to conduct the spatiotemporal analysis of forest fires, and the analysis scales included provinces and prefectural cities (districts and counties of Chongqing Municipality). The probability of forest fire pixels occurring in different regions was quantitatively assessed by calculating the proportion of forest fire pixels among all forest pixels in a region [46]. The formula for this calculation is given as follows:

$$P_{\text{re}} = \frac{N_{\text{fire}}}{N_{\text{forest}}} \tag{4}$$

$$P_{\text{Pro}} = \frac{\sum_{i=1}^{k} N_{\text{fire}_i}}{\sum_{i=1}^{k} N_{\text{forest}_i}} \tag{5}$$

where N_{fire_i} and N_{forest_i} are the numbers of forest fire and forest pixels in a prefecture (districts and counties), and P_{re} and P_{pro} denote the probability of forest fire in a prefecture and province, respectively.

2) Nearest-Neighbor Analysis: To investigate the impact of human activities on the spatial patterns of forest fires, nearest-neighbor analysis was employed to ascertain the distance from each forest fire pixel to its nearest stable light pixel [47]. This analytical method quantifies the minimal distance between points, providing information on the spatial distribution patterns and tendencies for spatial clustering. Geographic coordinates for both forest fire and stable light pixels were derived through the rectification and alignment of classification outcomes. In this study, the Euclidean distance calculation formula was used to calculate the shortest distance. This formula is given as follows:

$$d_{\text{min}}(p_1) = \min_{p_2 \in P_2} (D(p_1, p_2)) \tag{6}$$

where $d_{\text{min}}(p_1)$ denotes the shortest distance from a pixel p_1 (forest fire pixel) in set P_1 to the nearest pixel p_2 (stabilized light pixel) in set P_2; P_1denotes the set of all forest fire pixels; P_2 denotes the set of all stabilized light pixels; and Dp_1, p_2 are the Euclidean distances from pixel p_1 to pixel p_2.

IV. Results and Discussion

A. Accuracy Testing for Forest Fire Identification

We employed the random forest classification model to categorize NTL pixels across five provinces in Southwest China, utilizing VNP46A2 products from the years 2021 to 2022. By computing the average values of the attributes for black pixels, stable light pixels, and forest fire pixels from the chosen training samples of 2021 and 2022, as presented in Tables III and IV, it was observed that the peak NTL radiance for black pixels was substantially lower compared with the other two types of pixels. In addition, the proportion of NTL radiance greater than the threshold was significantly higher for stable light pixels, and the mutation rate of NTL radiance was markedly higher for forest fire pixels than for the other two types, demonstrating the efficacy of the feature calculation methodology in this research for differentiating between the three categories of pixels.

Utilizing the randomly selected samples, a confusion matrix was constructed for the screened valid samples for the years 2021 and 2022. As indicated in Tables V, VI, and VII, the classification efficacy of the three types of pixels demonstrates

TABLE III
Mean Value of Three Types of Pixels in 2021

Pixel Class	Maximum NTL Radiance (nW/cm²/sr)	Proportion of NTL Radiance Greater than Threshold (%)	Mutation Rate of NTL Radiance
Black Pixels	0.75	0.38	0.17
Stable Light Pixels	18.51	99.01	0.27
Forest Fire Pixels	44.46	2.41	62.12

TABLE IV
Mean Value of Three Types of Pixels in 2022

Pixel Class	Maximum NTL Radiance (nW/cm²/sr)	Proportion of NTL Radiance Greater than Threshold (%)	Mutation Rate of NTL Radiance
Black Pixels	0.81	0.00	0.13
Stable Light Pixels	18.15	98.41	0.28
Forest Fire Pixels	34.26	2.60	40.37

TABLE V
Confusion Matrix of Classification Results in 2021

	Black Pixels	Stable Light Pixels	Forest Fire Pixels	Producer Accuracy (%)
Black Pixels	489	11	0	97.80
Stable Light Pixels	0	496	1	99.80
Forest Fire Pixels	1	91	391	80.95
User Accuracy (%)	99.80	82.94	99.74	92.97

TABLE VI
CONFUSION MATRIX OF CLASSIFICATION RESULTS IN 2022

	Black Pixels	Stable Light Pixels	Forest Fire Pixels	Producer Accuracy (%)
Black Pixels	493	7	0	98.60
Stable Light Pixels	29	470	1	94.00
Forest Fire Pixels	0	48	452	90.40
User Accuracy (%)	94.44	89.52	99.78	94.33

TABLE VII
CLASSIFICATION ACCURACY OF DIFFERENT MACHINE LEARNING MODELS

Year	Random Forest	XGBoost	AdaBoost	K-NN
2021	93.3%	90.7%	79.46%	90.3%
2022	94.3%	90.3%	66.53%	83.9%
Average Accuracy	93.8%	90.5%	73.0%	87.1%

the model's considerable accuracy, with the overall pixel classification accuracies of 92.97% and 94.33% for 2021 and 2022, respectively. Black pixels achieved a higher producer accuracy, with rates of 97.8% and 98.6% for 2021 and 2022, respectively, while forest fire pixels attained a higher user accuracy, with rates of 99.74% and 99.78%. Nevertheless, diminished data accuracy due to light pollution in the vicinity of fires or proximate human activities could obscure the spectral signatures of the fire source in NTL images. This obscurity can lead to the conflation of characteristics between forest fire pixels and stable light pixels, culminating in lower producer accuracies for forest fire pixels at 80.95% and 90.40%.

B. Comparisons of Different Models for Forest Fire Identification

Leveraging SNPP-VIIRS data, the forest fire identification calculation results of the random forest classification model were compared with those of the K-NN, XGBoost, and AdaBoost classification models. According to Table VII, the random forest classification model's accuracy for the years 2021 and 2022 was recorded at 93.3% and 94.3%, respectively, with an average accuracy of 93.8% across both years. This surpasses the accuracies of the XGBoost model at 90.5%, the AdaBoost model at 73.0%, and the K-NN model at 87.1%. The random forest classification model exhibited enhanced stability, evidenced by consistent performance improvements and reduced accuracy fluctuations over the two-year period. In contrast, the other three machine learning

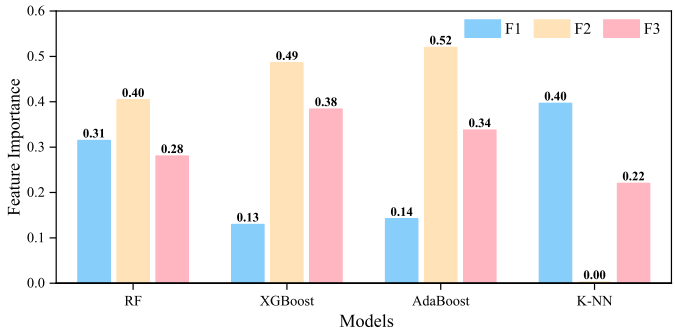

Fig. 6. Importance of features calculated by different machine learning models.

models demonstrated a downward trend in accuracy. The random forest classification model also showed superior generalization capabilities and adaptability to novel data. During forest fire detection, external factors, such as meteorological variations and anthropogenic activities, can introduce data anomalies. The robustness of the random forest classification model enables it to manage data irregularities more effectively, thereby diminishing the likelihood of overfitting and offering more dependable and generalizable predictive insights.

The evaluation of four machine learning models was deepened by contrasting the averaged importance values of each feature computed by the respective classification models across 2021 and 2022. Since the K-NN model itself cannot directly calculate feature importance, we introduced the permutation importance method to evaluate feature importance. Permutation importance estimates the importance of a feature by disrupting its value to disconnect the feature from the model output and then measuring the degradation of the model's performance after the disruption. As can be seen in Fig. 6, the random forest classification model has a relatively balanced distribution of importance on the three features (F_1, F_2, and F_3) and can consider multiple aspects of the data simultaneously for a more comprehensive analysis compared with other models. The other three models can over- or underemphasize certain features, which may lead to the model prediction relying too heavily on one feature or failing to reclassify the information obtained from using all the features.

C. Comparisons of Different Data for Forest Fire Identification

The forest fire identification results from the VNP46A2 NTL images are compared with four different fire point products that are widely used in fire monitoring, namely the MODIS, VIIRS (visible MODIS), and VIIRS active fire products produced by NASA, and the NPP nighttime fire products produced by the EOG. These are the main products used for the real-time monitoring and analysis of fire situations on the ground, for example, forest fires, agricultural fires, and grassland fires. Both MODIS and VIIRS deliver timely data on active fires, with the NOAA-20 and NPP satellites serving as critical sensors for global nighttime fire surveillance. Specifically, VIIRS discerns active fires with a 375 m resolution and is integral to the Suomi NPP and NOAA-20 missions. EOG leverages NTL observations

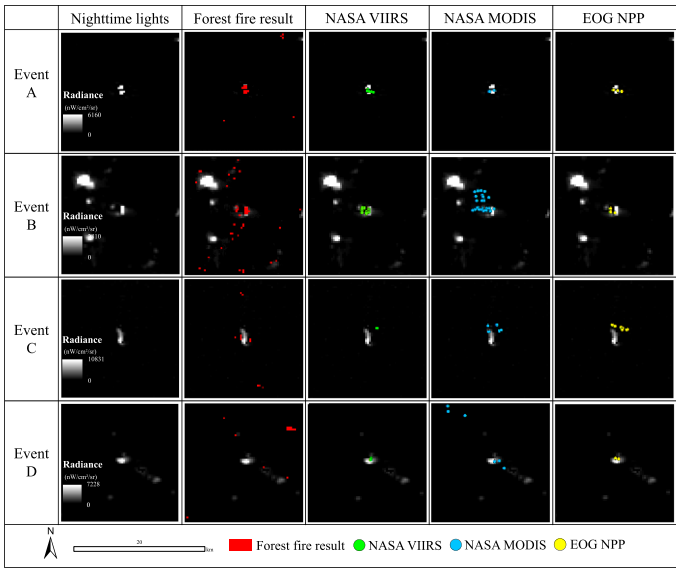

Fig. 7. Detection of forest fire pixels with fire products near typical fire events.

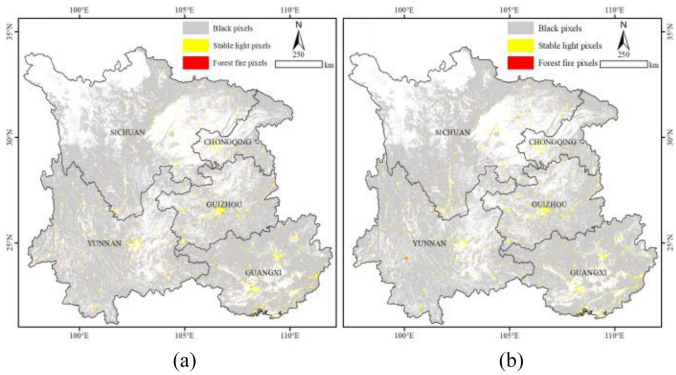

Fig. 8. Classification results for five provinces in Southwestern China. (a) 2021. (b) 2022.

TABLE VIII
CLASSIFICATION STATISTICS OF FIVE PROVINCES IN SOUTHWEST CHINA IN 2021

Province	Proportion of black pixels (%)	Proportion of stable light pixels (%)	Proportion of forest fire pixels (%)
Sichuan	97.49	2.07	0.44
Chongqing	95.27	4.09	0.63
Guizhou	94.32	4.90	0.78
Guangxi	94.06	4.82	1.12
Yunnan	96.55	2.70	0.76

to identify and exclude NTL irregularities, such as fires, thus refining the monitoring of urban expansion and changes in surface NTLs over time.

In this study, five typical fires were selected for the selection of cases: four typical major forest fires in the southwest region were selected as Event A: 22 February 2021, forest fire in Zian Village, Qinglian Town, Fengjie County, Chongqing Municipality; Event B: 20 April 2021, forest fire in Shilong Town, Coronation County, Liangshan Prefecture, Sichuan Province; Event C: 16 February 2022 forest fire in Hot, Glutinous Village, Gul Town, Jiulong County, Ganzi Prefecture, Sichuan Province; and Event D: 3 March 2022, forest fire in Pingtang County, Qiandang Prefecture, Guizhou Province. Kukou forest fire, and Event D: 3 March 2022, forest fire in Pingtang County, Qiannan Prefecture, Guizhou Province. The pixels were selected from the VNP46A2 NTL imagery, GlobeLand30 ground cover data, and Google Earth imagery based on the records of the five typical forest fire events. The forest fire pixels were effectively identified by combining the forest conditions on the Google Earth imagery as well as by ensuring that the proportion of the ground cover type of the pixel interior was forested land was greater than 20%.

Fig. 7 shows the NTL images, forest fire recognition results, and the three types of fire point products near the area of four typical forest fires. The results show that the forest fire pixel recognition results are better and correspond to those of the other three fire products. In contrast to the three types of fire point products, NTL images can capture open fires at night and more sensitively detect light sources caused by fires. Forest fires are subject to a variety of factors in the wild environment, such as wind speed and vegetation type, that can affect the flame temperature, which limits temperature-based fire detection. In contrast, forest fire pixel recognition with NTL images is able to recognize flames that are still visible despite lower temperatures.

D. Characterization of Spatiotemporal Distribution of Forest Fires in Southwest China in 2021 and 2022

Fig. 8 shows the classification results for five provinces in Southwest China. We calculated the proportion of black pixels, stable light pixels, and forest fire pixels in each province. From Tables VIII and IX, it can be seen that the proportion of black pixels is the largest in all five provinces, followed by stabilized light pixels and, finally, forest fire pixels. The largest percentage of forest fire pixels in 2021 is in Guangxi province, followed by Guizhou province, and the largest percentage of forest fire pixels in 2022 is in Guangxi province, followed by Yunnan province. The proportion of forest fire pixels is related to the special climatic conditions and anthropogenic activities in each region in different years. While the proportion of forest fire pixels generally decreased from 2021 to 2022, this change may be caused by climatic factors, such as relatively mild climatic conditions and sufficient precipitation in each province in 2022, as well as by effective national forest fire prevention measures, the implementation of forest management policies, and the improvement in fire emergency response capacity.

By calculating the probability of forest fires in prefectures in each province (adopting districts and counties in Chongqing),

TABLE IX
CLASSIFICATION STATISTICS OF FIVE PROVINCES IN SOUTHWEST CHINA IN 2022

Province	Proportion of black pixels (%)	Proportion of stable light pixels (%)	Proportion of forest fire pixels (%)
Sichuan	97.49	2.07	0.44
Chongqing	95.27	4.09	0.63
Guizhou	94.32	4.90	0.78
Guangxi	94.06	4.82	1.12
Yunnan	96.55	2.70	0.76

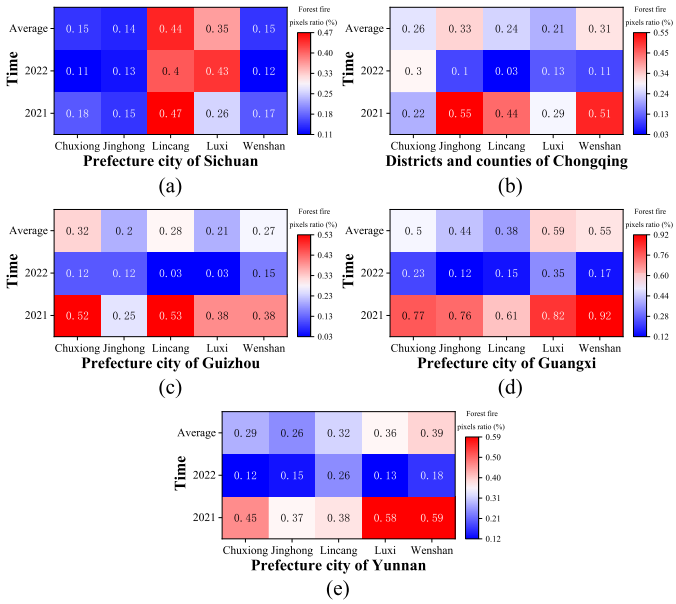

Fig. 9. Forest fire risk heat map. (a) Sichuan. (b) Chongqing. (c) Guizhou. (d) Guangxi. (e) Yunnan.

the top five prefectures (districts and counties) with the highest probability in each province were screened to produce heat maps (see Fig. 9). The results show that the probability of forest fires in 2022 decreased significantly in most of the cities compared with 2021, and an increase was only shown in individual cities, such as Suining City in Sichuan Province. The heat map can effectively visualize high-risk areas for forest fires in the southwestern provinces, such as Panzhihua City in Sichuan Province, Wuzhou City in Guangxi Province, and Wenshan City in Yunnan Province. The accurate identification of high-risk areas for fires can lead to a reassessment of the regional allocation of fire prevention resources and management measures in order to reduce the potential risk of forest fires.

The distribution map of the three types of pixel results shows that the distribution of forest fires in Southwest China is not

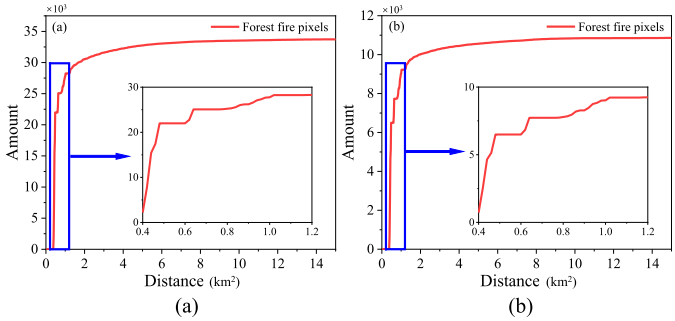

Fig. 10. Cumulative distribution of nearest-neighbor distances from forest fire pixels to stable light pixels. (a) 2021. (b) 2022.

significantly concentrated in one region. There are numerous scattered fire points, which do not form a large continuous fire area. Fig. 10 shows the cumulative distribution statistics of forest fire pixels to the nearest-neighboring stable light pixels in Southwest China from 2021 to 2022. The results indicate that forest fire pixels are predominantly distributed around stable light pixels, mainly clustering within a range of 400–700 m. Stable light pixels are more commonly found in towns and their surrounding areas; these are regions of intense human activity encompassing agricultural farming, logging, residential areas, etc. Many of the causes of forest fires are directly related to human activity, such as intentional or unintentional fire placement, agricultural cleaning of the land, and inappropriate treatment of campfires. Thus, the concentrated distribution of forest fire pixels around stable light pixels indicates that populated areas can significantly increase the forest fire risk. Overall, forest fire activity showed a decreasing trend in 2022 compared with 2021; this provides important reference information for the development of further forest management strategies and forest protection efforts.

E. Limitations and Future Research Directions

The SNPP-VIIRS data used to identify the three types of pixels this study was partially missing due to problems with the data source. To deal with day-level data with missing slices, we averaged the data obtained from adjacent days. Data with greater missing time periods, such as the 26 July and 10 August data in 2022, were excluded from this study. In addition, despite the superior performance of random forest classification, it cannot handle noisy data or outliers well and is prone to overfitting when modeling data. Therefore, we used low-dimensional data with fewer categorical features, which are easier to classify. In future research, we can explore multimodal data fusion methods, such as combining ground monitoring station data and multisource satellite images, to improve the accuracy of forest fire detection. In addition, we can consider employing more complex machine learning models, such as deep learning algorithms, to classify and recognize the data more effectively, thereby addressing the complexity of forest fire data.

V. Conclusion

In this study, Southwest China was used as the study area and constructed radiance multivariate features using the black marble day-level NTL imagery VNP46A2 product. The NTL pixels in the forest region were classified into black pixels, stable light pixels, and forest fire pixels using the random forest classification model, and the overall classification accuracy, producer accuracy, and user accuracy of the pixel classifications were calculated after accuracy validation. The results of random forest classification were analyzed and compared with those of the K-NN, XGBoost, and AdaBoost machine learning models to verify that random forest classification is the optimal model for forest fire pixel recognition. The classification prediction results were compared with three different fire point product data to verify that the forest fire pixel identification results were more reliable. The spatiotemporal analysis of the forest fire identification results shows that the distribution of forest fires in Southwest China is more scattered in 2021 and 2022, mainly around human activity areas of 400–700 m in forests, and that the distribution of forest fires was significantly reduced in 2022 compared with 2021. A dataset of forest fires in Southwest China in 2021 and 2022 was successfully constructed using machine learning models. This not only provides a scientific basis for forest fire monitoring and prevention in Southwest China but also provides a new perspective for elucidating the complex relationship between forest fires and environmental factors. At the same time, it provides a basis for further scientific research addressing global ecological security and the sustainable development goals, and holds promise for future forest fire management and decision support.

References

[1] P. M. Brown, C. Gentry, and Q. Yao, "Historical and current fire regimes in ponderosa pine forests at Zion National Park, Utah: Restoration of pattern and process after a century of fire exclusion," *Forest Ecol. Manage.*, vol. 445, pp. 1–12, 2019.

[2] E. Chuvieco, L. Giglio, and C. Justice, "Global characterization of fire activity: Toward defining fire regimes from Earth observation data," *Glob. Change Biol.*, vol. 14, no. 7, pp. 1488–1502, 2008.

[3] F. Ahmad and L. Goparaju, "Forest fire trend and influence of climate variability in India: A geospatial analysis at national and local scale," *Ekológia*, vol. 38, no. 1, pp. 49–68, 2019.

[4] E. Chuvieco et al., "Historical background and current developments for mapping burned area from satellite Earth observation," *Remote Sens. Environ.*, vol. 225, pp. 45–64, 2019.

[5] L. Ying, J. Han, Y. Du, and Z. Shen, "Forest fire characteristics in China: Spatial patterns and determinants with thresholds," *Forest Ecol. Manage.*, vol. 424, pp. 345–354, 2018.

[6] D. McKenzie et al., "Smoke consequences of new wildfire regimes driven by climate change," *Earth's Future*, vol. 2, no. 2, pp. 35–59, 2014.

[7] M. Hamilton, A. P. Fischer, S. D. Guikema, and G. Keppel-Aleks, "Behavioral adaptation to climate change in wildfire-prone forests," *WIREs Climate Change*, vol. 9, no. 6, 2018, Art. no. e553.

[8] J. Sobrino, R. Llorens, C. Fernández, J. Fernández-Alonso, and J. Vega, "Relationship between soil burn severity in forest fires measured in situ and through spectral indices of remote detection," *Forests*, vol. 10, no. 5, 2019, Art. no. 457.

[9] L. Aragao et al., "21st century drought-related fires counteract the decline of Amazon deforestation carbon emissions," *Nature Commun.*, vol. 9, no. 1, Feb. 2018, Art. no. 536.

[10] C. E. Gordon, O. F. Price, and E. M. Tasker, "Mapping and exploring variation in post-fire vegetation recovery following mixed severity wildfire using airborne LiDAR," *Ecol. Appl.*, vol. 27, no. 5, pp. 1618–1632, Jul. 2017.

[11] F. Alimenti et al., "A low-cost microwave radiometer for the detection of fire in forest environments," *IEEE Trans. Geosci. Remote Sens.*, vol. 46, no. 9, pp. 2632–2643, Sep. 2008.

[12] D. Szpakowski and J. Jensen, "A review of the applications of remote sensing in fire ecology," *Remote Sens.*, vol. 11, no. 22, 2019, Art. no. 2638.

[13] E. Chuvieco, I. Aguado, J. Salas, M. García, M. Yebra, and P. Oliva, "Satellite remote sensing contributions to wildland fire science and management," *Curr. Forestry Rep.*, vol. 6, no. 2, pp. 81–96, 2020.

[14] N. Levin et al., "Remote sensing of night lights: A review and an outlook for the future," *Remote Sens. Environ.*, vol. 237, 2020, Art. no. 111443.

[15] S. Liu, K. Shi, and Y. Wu, "Identifying and evaluating suburbs in China from 2012 to 2020 based on SNPP–VIIRS nighttime light remotely sensed data," *Int. J. Appl. Earth Observ. Geoinf.*, vol. 114, 2022, Art. no. 103041.

[16] K. Shi, J. Ma, Z. Chen, Y. Cui, and B. Yu, "Nighttime light remote sensing in characterizing urban spatial structure," *Innov. Geosci.*, vol. 1, no. 3, 2023, Art. no. 100043.

[17] K. Shi, Y. Wu, S. Liu, Z. Chen, C. Huang, and Y. Cui, "Mapping and evaluating global urban entities (2000–2020): A novel perspective to delineate urban entities based on consistent nighttime light data," *GIScience Remote Sens.*, vol. 60, no. 1, 2023, Art. no. 2161199.

[18] K. Shi, B. Yu, J. Ma, W. Cao, and Y. Cui, "Impacts of slope climbing of urban expansion on global sustainable development," *Innovation*, vol. 4, no. 6, Nov. 2023, Art. no. 100529.

[19] P. Jain, S. C. P. Coogan, S. G. Subramanian, M. Crowley, S. Taylor, and M. D. Flannigan, "A review of machine learning applications in wildfire science and management," *Environ. Rev.*, vol. 28, no. 4, pp. 478–505, 2020.

[20] R. Gibson, T. Danaher, W. Hehir, and L. Collins, "A remote sensing approach to mapping fire severity in south-eastern Australia using sentinel 2 and random forest," *Remote Sens. Environ.*, vol. 240, 2020, Art. no. 111702.

[21] M. Belgiu and L. Drăguţ, "Random forest in remote sensing: A review of applications and future directions," *ISPRS J. Photogramm. Remote Sens.*, vol. 114, pp. 24–31, 2016.

[22] F. Huot, R. L. Hu, N. Goyal, T. Sankar, M. Ihme, and Y.-F. Chen, "Next day wildfire spread: A machine learning dataset to predict wildfire spreading from remote-sensing data," *IEEE Trans. Geosci. Remote Sens.*, vol. 60, Art. no. 4412513.

[23] S. Park, J. Im, S. Park, C. Yoo, H. Han, and J. Rhee, "Classification and mapping of paddy rice by combining Landsat and SAR time series data," *Remote Sens.*, vol. 10, no. 3, 2018, Art. no. 447.

[24] S. Asadollah, A. Sharafati, and D. Motta, "Satellite-based ensemble intelligent approach for predicting forest fire: A case of the Hyrcanian forest in Iran," *Environ. Sci. Pollut. Res.*, vol. 31, pp. 22830–22846, Feb. 2024.

[25] A. S. Kulinan, Y. Cho, M. Park, and S. Park, "Rapid wildfire damage estimation using integrated object-based classification with auto-generated training samples from Sentinel-2 imagery on Google Earth engine," *Int. J. Appl. Earth Observ. Geoinf.*, vol. 126, 2024, Art. no. 103628.

[26] K. Mehmood et al., "Assessing chilgoza pine (pinus gerardiana) forest fire severity: Remote sensing analysis, correlations, and predictive modeling for enhanced management strategies," *Trees, Forests People*, vol. 16, 2024, Art. no. 100521.

[27] B. Bechtel and C. Daneke, "Classification of local climate zones based on multiple Earth observation data," *IEEE J. Sel. Topics Appl. Earth Observ. Remote Sens.*, vol. 5, no. 4, pp. 1191–1202, Aug. 2012.

[28] H. K. Zhang and D. P. Roy, "Using the 500 m MODIS land cover product to derive a consistent continental scale 30 m Landsat land cover classification," *Remote Sens. Environ.*, vol. 197, pp. 15–34, 2017.

[29] Y. Sun, Q. Zhang, K. Li, Y. Huo, and Y. Zhang, "Trace gas emissions from laboratory combustion of leaves typically consumed in forest fires in Southwest China," *Sci. Total Environ.*, vol. 846, Nov. 2022, Art. no. 157282.

[30] K. Luo, X. Quan, B. He, and M. Yebra, "Effects of live fuel moisture content on wildfire occurrence in fire-prone regions over southwest China," *Forests*, vol. 10, no. 10, 2019, Art. no. 887.

[31] R. H. Nolan, M. M. Boer, V. Resco de Dios, G. Caccamo, and R. A. Bradstock, "Large-scale, dynamic transformations in fuel moisture drive wildfire activity across southeastern Australia," *Geophysical Res. Lett.*, vol. 43, no. 9, pp. 4229–4238, 2016.

[32] Z. Wang, M. O. Román, V. L. Kalb, S. D. Miller, J. Zhang, and R. M. Shrestha, "Quantifying uncertainties in nighttime light retrievals from Suomi-NPP and NOAA-20 VIIRS day/night band data," *Remote Sens. Environ.*, vol. 263, 2021, Art. no. 112557.

[33] Y. Tang, Z. Shao, X. Huang, and B. Cai, "Mapping impervious surface areas using time-series nighttime light and MODIS imagery," *Remote Sens.*, vol. 13, no. 10, 2021, Art. no. 1900.

[34] T. Li, Z. Zhu, Z. Wang, M. O. Román, V. L. Kalb, and Y. Zhao, "Continuous monitoring of nighttime light changes based on daily NASA's black marble product suite," *Remote Sens. Environ.*, vol. 282, 2022, Art. no. 113269.
[35] C. Jun, Y. Ban, and S. Li, "China: Open access to Earth land-cover map," *Nature*, vol. 514, no. 7523, Oct. 2014, Art. no. 434.
[36] H. Cao, Y. Wang, X. Li, S. Hu, S. Qiu, and Y. Wei, "Detecting farmland fire in VIIRS night-time light images," Wuhan Univ., Wuhan, China, 2023, pp. 1–19.
[37] L. Breiman, "Random forests," *Mach. Learn.*, vol. 45, no. 1, pp. 5–32, 2001.
[38] T. Chen and C. Guestrin, "XGBoost," in *Proc. 22nd ACM SIGKDD Int. Conf. Knowl. Discov. Data Mining*, 2016, pp. 1–4.
[39] W. S. Cleveland and S. J. Devlin, "Locally weighted regression: An approach to regression analysis by local fitting," *J. Amer. Statist. Assoc.*, vol. 83, no. 403, pp. 596–610, 1988.
[40] H. Franco-Lopez, A. R. Ek, and M. E. Bauer, "Estimation and mapping of forest stand density, volume, and cover type using the k-nearest neighbors method," *Remote Sens. Environ.*, vol. 77, no. 3, pp. 251–274, 2001.
[41] Y. Freund and R. E. Schapire, "A decision-theoretic generalization of on-line learning and an application to boosting," *J. Comput. Syst. Sci.*, vol. 55, no. 1, pp. 119–139, 1997.
[42] L. Giglio, W. Schroeder, and C. O. Justice, "The collection 6 MODIS active fire detection algorithm and fire products," *Remote Sens. Environ.*, vol. 178, pp. 31–41, Jun. 2016.
[43] W. Schroeder, P. Oliva, L. Giglio, and I. A. Csiszar, "The new VIIRS 375 m active fire detection data product: Algorithm description and initial assessment," *Remote Sens. Environ.*, vol. 143, pp. 85–96, 2014.
[44] M. Jiao, X. Quan, and J. Yao, "Evaluation of four satellite-derived fire products in the fire-prone, cloudy, and mountainous area over sub-tropical China," *IEEE Geosci. Remote Sens. Lett.*, vol. 19, Jul. 2022, Art. no. 6513405.
[45] Y. Liu, C. Hu, W. Zhan, C. Sun, B. Murch, and L. Ma, "Identifying industrial heat sources using time-series of the VIIRS nightfire product with an object-oriented approach," *Remote Sens. Environ.*, vol. 204, pp. 347–365, 2018.
[46] J. R. Gonzalez-Olabarria, B. Mola-Yudego, T. Pukkala, and M. Palahi, "Using multiscale spatial analysis to assess fire ignition density in Catalonia, Spain," *Ann. Forest Sci.*, vol. 68, no. 4, pp. 861–871, 2011.
[47] Z. Xia, H. Li, Y. Chen, and W. Yu, "Detecting urban fire high-risk regions using colocation pattern measures," *Sustain. Cities Soc.*, vol. 49, 2019, Art. no. 101607.

Yuehan Yu is currently working toward the B.S. degree in geographic information science with the School of Geographical Sciences, Southwest University, Chongqing, China.

Her research interests include nighttime light remote sensing and urban geography.

Lili Liu is currently working toward the M.S. degree in geographic information science with the School of Geographical Sciences, Southwest University, Chongqing, China.

Her research interests include nighttime light remote sensing and urban geography.

Zhijian Chang is currently working toward the M.S. degree in geographic information science with the School of Geographical Sciences, Southwest University, Chongqing, China.

His research interests include nighttime light remote sensing and urban geography.

Yuanqing Li received the Ph.D. degree in physical geography from Southwest University, Chongqing, China, in 2022.

He is currently an Office Director of Chongqing Jinfo Mountain Karst Ecosystem National Observation and Research Station, School of Geographical Sciences, Southwest University, Chongqing, China. His research interests include spatial planning, land resources, and regional development research.

Kaifang Shi (Member, IEEE) received the Ph.D. degree in cartography and geographic information systems from East China Normal University, Shanghai, China, in 2017.

He is currently a Professor with the School of Geography and Tourism, Anhui Normal University, Wuhu, China. His research interests include remote sensing analysis in socioeconomic characterization and urbanization process, nighttime light remote sensing, and urban geography.